Journal of Computational Physics **154,** 245–265 (1999)
Article ID jcph.1999.6302, available online at http://www.idealibrary.com on IDEAL®

Hybrid Atomistic–Continuum Formulations and the Moving Contact-Line Problem

Nicolas G. Hadjiconstantinou

Department of Mechanical Engineering, Massachusetts Institute of Technology, Cambridge, Massachusetts 02139

Received March 11, 1999

We present a hybrid atomistic–continuum computational framework for the treatment of dense fluid problems with emphasis on the coupling of molecular dynamics with continuum (finite element/spectral) methods for problems involving multi-fluid dynamics in the presence of multi-fluid interfaces. The technique is an extension of the single-fluid framework already presented by the author. The well-known moving contact-line problem is used as a validation example. A hybrid solution that employs molecular dynamics close to the walls where molecular effects are important and continuum fluid mechanics in the remainder of the domain (far field region) is obtained. A fully molecular solution of the same problem serves as an exact solution. Various issues related to dense fluid atomistic–continuum techniques are discussed and contrasted to the already existing but less general dilute gas techniques. Numerical considerations are discussed with particular emphasis on efficiency, and a formulation that reduces computational cost is proposed. © 1999 Academic Press

Key Words: hybrid formulation; molecular dynamics; coupling.

1. INTRODUCTION

1.1. *Background*

Despite the enormous success enjoyed by computer modeling at the molecular scale, the computational profligacy of the various techniques employed does not allow the satisfactory treatment of fully macroscopic problems. As a result, molecular modeling is used in a "sequential" atomistic *then* continuum fashion, which usually means that continuum treatments use molecular information indirectly in the form of constitutive relations and laws developed from molecular studies. Researchers [1–7] have realized that hybrid techniques may, in some cases, alleviate this significant limitation inherent in molecular simulation techniques.

Hybrid techniques can be very effective in reducing the computational cost of a numerical solution by limiting the use of the molecular treatment to the regions where it is essential

0021-9991/99 $30.00
Copyright © 1999 by Academic Press
All rights of reproduction in any form reserved.

(mainly due to the inapplicability of the more conventional continuum techniques), and use the significantly less computationally expensive continuum techniques in the majority of the computational domain. The computational gain depends on the size of the continuum relative to the molecular regions, the size of the overlap region usually used to "interface" the two descriptions, and the relative speed of the numerical implementations of the two descriptions. We will limit our discussion here to the development of hybrid techniques for fluid mechanics, and more specifically we focus on dense fluids that require molecular dynamics (MD) for their correct treatment. Previous work on hybrid techniques for dense fluids is limited to the technique by O'Connel and Thompson [5]. Their technique, however, does not decouple timescales and a simple estimate shows that for a given problem it can be $O(100)$ times slower than the present technique which decouples timescales. Timescale decoupling is discussed in Section 1.3. Some discussion on hybrid techniques for solid mechanics can be found in [1, 6].

When molecular dynamics provides the molecular modeling, only very small regions can be treated; the potential savings from the use of a hybrid technique in this case can be enormous. However, a problem is amenable to simulation by hybrid techniques only if the region that requires treament by MD is localized and of small spatial extent such that its simulation by MD is feasible. An example of such a problem is the moving contact-line problem [8, 9]. It has long been concluded that the correct treatment of the moving contact-line problem requires modeling at the atomistic scale; the main obstacle to the successful continuum simulation of this problem is the inability to approximate with continuum equations the molecular dynamics governing the continuum behavior of the contact line. The author has shown [10] that the microscale treatment required can be limited to distances of a few molecular diameters from the contact line, thus providing a good example for the application of a hybrid technique. We will use this problem as an example throughout this paper.

1.2. *The Hybrid Coupling Method*

The hybrid technique used in this paper is a modified version of the general method presented in [6] and its origins can be traced to the domain decomposition technique known as the Schwarz alternating method. Although this technique can be applied to an arbitrary number of subdomains, in what follows we assume that we have one MD and one continuum subdomain. Lengthscale decoupling is achieved through the use of an overlap region across which the continuum and molecular subdomains exchange information; it is, of course, assumed that both descriptions are valid in that region. The Schwarz technique is inherently a steady-state solution method; in fact, this is the reason it is able to decouple timescales as well as lengthscales. Transient problems are treated quasistatically: a series of Schwarz iterations is performed, one for each time step. Timescale decoupling is discussed in Section 1.3.

Iterative convergence to a (quasi-)steady solution is achieved through an alternating iteration between *steady-state* solutions in the two subdomains. If we denote the continuum and molecular subdomains as Ω_{cont} and Ω_{mol}, respectively, with Γ_{cont} and Γ_{mol} their respective boundaries, the iteration proceeds as follows: a *steady-state* solution in the continuum subdomain subject to "external" boundary conditions on Γ_{cont} excluding $(\Gamma_{\text{cont}} \cap \Omega_{\text{mol}})$, and "iterative" boundary conditions on $\Gamma_{\text{cont}} \cap \Omega_{\text{mol}}$ from the previous solution in Ω_{mol} provides new "iterative" boundary conditions on $\Omega_{\text{cont}} \cap \Gamma_{\text{mol}}$ for a new solution in Ω_{mol} subject also to "external" boundary conditions on Γ_{mol} excluding $(\Gamma_{\text{mol}} \cap \Omega_{\text{cont}})$. This iteration procedure continues until the solution in the overlap region is the same in both subdomains

which means that fluxes (=(transport coefficients) × (gradients)) are matched (under the assumption of matched transport coefficients in the two subdomains). The first solution in Ω_{cont} can be a guess or an approximate solution if available. Starting from solutions close to the exact one will, in general, reduce the number of iterations required but the technique is expected to converge from solutions arbitrarily far from the exact solution [11].

The author has previously [6] pointed out some issues related to a general hybrid MD–continuum simulation framework: these include the scaling relation between the MD domain data noise and domain sizes, the accurate imposition of Dirichlet boundary conditions and the role of the overlap region as a relaxation region for the non-equilibrium distribution function, and the extension of the Schwarz framework to treat complex fluid mechanical phenomena such as the moving contact-line problem. These issues are revisited and discussed below.

The first issue is related to the statistical nature of molecular dynamics: the need for adequate signal-to-noise ratio in every MD simulation usually results in unrealistically large gradients in the very small simulation domain. This, in turn, sets a limit on the size of the continuum computational domain since such gradients cannot persist over macroscopic distances. In other words, although a matching technique can be devised that can couple a molecular dynamics simulation domain to an arbitrarily large continuum domain, in order for a problem to be feasible, it would have to exhibit gradients that exceed the value of 10^7 by usually a few orders of magnitude and decay fast enough into the continuum region so as not to lead to diverging field variables (for example, a velocity gradient of 10^9 s^{-1} over a distance of 1 m results in a velocity that exceeds the speed of light!). It would seem that this issue can never be fully addressed, but only alleviated by the use of increased computational resources, thus seriously limiting the applicability of any hybrid technique irrespective of its ability to couple the various subdomains successfully. The author has indicated in [6] the use of dynamical similarity to overcome this problem: in situations that non-dimensional governing parameters do not place conflicting requirements, the molecular simulation can be performed on a dynamically and geometrically similar system with smaller characteristic dimensions (d) and higher characteristic field variables scales, such as velocity (v), to give a higher signal-to-noise ratio. As an example, consider a flow which is characterised by the Reynolds number ($\text{Re} = \rho v d/\mu$) only: this is an ideal situation because Re can be kept constant by increasing v and at the same time decreasing d, thus increasing the gradients (g) in the flow proportionally to the square of the characteristic velocity ($g \sim v/d \propto v^2$). Care must be taken in ensuring that this procedure does not change the relative importance of other controlling parameters which would lead to introduction of effects that are not present in the original model, such as viscous heating and shear thinning.

The second issue arises because of the non-local nature of fluxes (shear stress, heat flux) which as such are almost impossible to impose in a molecular dynamics simulation. We expect that successful matching of two solutions in two different subdomains implies the matching of these fluxes across the subdomain boundaries. This was most often cited as the major difficulty in obtaining a hybrid MD–continuum simulation technique [12]. The hybrid solution framework proposed by the author [6] overcomes this problem by providing an iterative technique that ensures that fluxes are correctly matched through the imposition of Dirichlet boundary conditions which are significantly easier to impose. Although the author has reported [6] some error resulting from the method used to impose the Dirichlet boundary conditions in MD simulations, this issue is not as important and it is the author's belief that it can be reasonably easily rectified.

The hybrid technique used here exhibits favorable convergence characteristics; the convergence rate depends primarily on the size of the overlap region relative to the smallest of the subdomains. As a result, an overlap region of the size of the molecular only region (Ω_{mol} excluding $\Omega_{\text{mol}} \cap \Omega_{\text{cont}}$) leads to a fast converging iteration irrespective of the size of the continuum domain which can be up to a few orders of magnitude larger (subject to the first issue discussed above). Convergence can be proven for elliptic problems [11], and as shown in Section 4, more efficient algorithms can be designed based on these convergence characteristics.

1.3. *Timescale Decoupling and Transient Problems*

The Schwarz alternating method was chosen for its ability to decouple timescales as well as lengthscales. The majority of previous work has been focused on the coupling of the direct simulation Monte Carlo (DSMC) to a continuum description. This choice, however, does not bring to surface two important obstacles in the way of obtaining a fully general hybrid description: the first obstacle is the imposition of fluxes which is not an issue in the DSMC (kinetic theory) framework because of the absence of interaction between molecules; the second obstacle is the decoupling of timescales, which is not as serious a limitation in the DSMC case due to the similarity of the timescales between DSMC and continuum formulations. It does, however, set an upper limit in the maximum scale separation that can be achieved even in the DSMC–continuum case.

More specifically, the molecular dynamics integration timestep (τ_{MD}) is a small fraction of the molecular collision frequency (τ_{c}). These characteristic times are much shorter than the hydrodynamic timescale of any system (τ_{h}), even for systems with a very small number of molecules. As a result, macroscopic phenomena evolving on macroscopic timescales cannot be captured by *any* technique that has an integration timescale of the order of τ_{MD} (such as a hybrid technique that does not decouple timescales), because of the enormous number of time steps required. As an example, consider a three-dimensional system of characteristic size $l \sim 10^{-6}$ m. The hydrodynamic scale for this system (assuming incompressible, low-speed flow) is $\tau_{\text{h}} \sim \tau_{\text{d}} \sim l^2/\nu$; here we have assumed that the Reynolds number $\text{Re} = \tau_{\text{d}}/\tau_{\text{i}} = vl/\nu$ is of order one, where τ_{d} is the momentum diffusion timescale, τ_{i} is the inertial timescale, ν is the kinematic viscosity, and v is a characteristic velocity. If we take $\nu \sim 10^{-7}\,\text{m}^2/\text{s}$, it follows that $\tau_{\text{h}} \sim 10^{-5}$ s or equivalently $\tau_{\text{h}} \sim 10^{9}\tau_{\text{MD}}$, which is already out of reach of most computers, even if we assume that through a hybrid technique we are only required to cover a small region of the original domain by MD (say $l_{\text{MD}} \sim 10^{-8}$ m). In DSMC the integration timescale $\tau_{\text{DSMC}} \gg \tau_{\text{MD}}$; in a sense DSMC achieves a form of timescale decoupling by "coarse-graining" the molecular description up to the level of the hydrodynamic regime. As a result, the above limitations are less restrictive for the case of a DSMC–continuum technique. Furthermore, the computational efficiency of DSMC (compared to MD) results in hybrid formulations which can approach the micrometer scale [7] before the separation of timescales seriously affects them.

Timescale decoupling is achieved here by treating steady-state problems in an implicit sense: the steady solution is obtained by an iteration sequence that has no temporal interpretation (much like a Gauss–Seidel iteration) and takes $O(10)$ steps. Time-varying problems require one Schwarz iteration per time step during which the solution is treated as steady. Using our example above, the numerical integration of a problem with characteristic timescale $\tau_{\text{h}} \sim 10^{-5}$ s will require an integration timescale $d\tau \sim 10^{-7}$ s. This, however,

is very long compared to the characteristic time of the MD region $\tau_{\mathrm{hMD}} \sim l_{\mathrm{MD}}^2/\nu \sim 10^{-9}$ s and hence a quasistatic treatment of the molecular region is justified. The technique presented is thus not limited to steady-state problems.

1.4. *Paper Overview*

As remarked above, this paper focuses on the extension of the hybrid technique to treat a realistic example that is both a challenging test for the hybrid framework and of practical importance and interest. The description of the moving contact-line example problem, the molecular simulation of the same problem which provides the exact solution for comparison purposes but also provides the molecular part of the hybrid solution, and the continuum simulation technique used are presented in the next section; the hybrid formulation and its results are presented in Section 3, various numerical considerations are discussed in Section 4, and some concluding remarks are given in Section 5.

2. THE MOVING CONTACT-LINE PROBLEM

2.1. *Problem Description*

In this paper we study a simple version of the moving contact-line problem. Consider first two static immiscible but otherwise identical fluids (same density (ρ) and viscosity (μ)) in a two-dimensional channel: the meniscus that separates the two fluids will adopt a shape that balances the capillary stresses with the pressure difference between the two fluids, subject to the (static) contact-angle boundary condition. We next permit the two fluids to move. In particular, we consider the problem in which one fluid displaces the other fluid at a constant interface (average fluid displacement) speed U. This movement is a result of boundary forcing which takes place at the expense of a pressure drop along the direction of motion, or a result of an external field (such as gravity) acting along the direction of motion. The meniscus shape will now further distort due to the stresses created by the flowing fluid; the interface shape is an unknown and must be determined with the flow field by solution of a non-linear set of coupled partial differential equations. The problems of interest here are limited to the case of small Reynolds number, $\mathrm{Re} \equiv \rho U H/\mu \ll 1$, and small capillary number, $\mathrm{Ca} \equiv \mu U/\gamma < 0.1$; here ρ is the density, H is the channel half-width, μ is the dynamic viscosity, and γ is the assumed-constant coefficient of surface tension between the two fluids.

It is convenient to study this problem in the reference frame of the moving interface (see Fig. 1): in this reference frame the interface does not move, and the walls of the channel move with speed $-U$ (where U is the speed with which the interface advances in the laboratory frame) in the streamwise direction.

The numerical solution of this problem presents various challenges, both numerical and theoretical, mainly due to the insufficient understanding of the dynamics of the contact point (point H in Fig. 1). The conflicting requirements of the no-slip condition, which requires the fluid in contact with the wall to acquire the wall velocity ($-U$) in the direction along the wall, and the so-called kinematic condition, which requires no net mass flux through a two-fluid interface and thus zero fluid velocity in the streamwise direction at the contact point, leads to a logarithmic stress singularity at the contact point [8]. This singularity is relieved in numerical treatments through the introduction of slip models with adjustable parameters that are, however, ad hoc. The value of the contact angle θ at H (dynamic in the

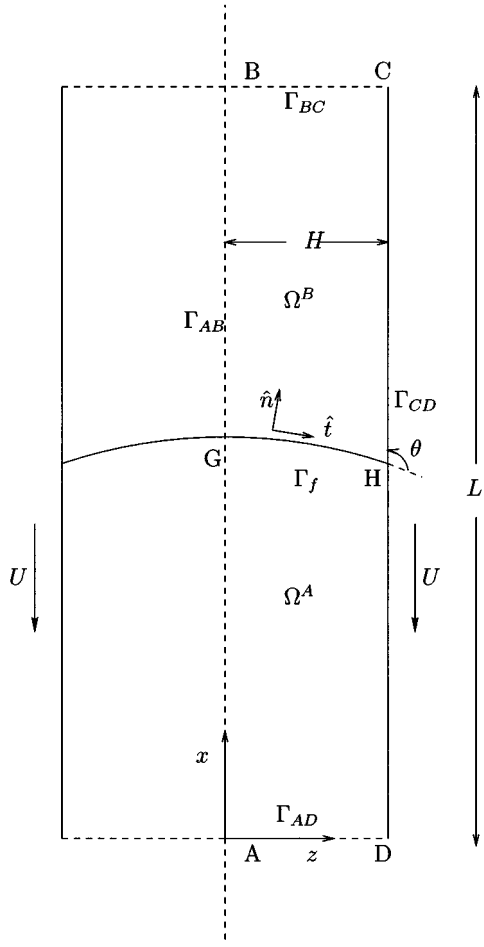

FIG. 1. Schematic of the moving contact-line example problem. We use Γ to denote the various boundaries of the system. The system is symmetric about the channel centerline Γ_{AB}. The two-fluid interface (Γ_{f}) is denoted GH, where H is the contact point (two-dimensional projection of the contact line). The two fluid domains are denoted Ω^A and Ω^B.

case of a moving wall) as a function of the wall velocity is another unknown. This angle is required as a boundary condition for the integration of the governing equations of motion. Agreement with experiments can be obtained by using the value of the dynamic contact angle and the slip parameters as adjustable parameters. This, however, is not satisfactory from a theoretical point of view which requires a model of the contact-line dynamics to be predictive. The complex molecular-kinetic contact-line dynamics can be adequately captured by molecular simulations [9, 10, 12–14]. We thus propose a hybrid solution of the problem with the region close to the walls, region L′U′CD in Fig. 2, being treated by molecular dynamics, and region ABU″L″ in Fig. 2 being treated by continuum theory. Note that L′U′U″L″ is an overlap region where both descriptions are assumed to be valid.

The objective of this study is the evaluation of the ability of the hybrid technique proposed in [6] to capture the complex multi-dimensional dynamics of multi-fluid flows. The contact-line problem is a very stringent test for our technique; the resulting flow field is extremely

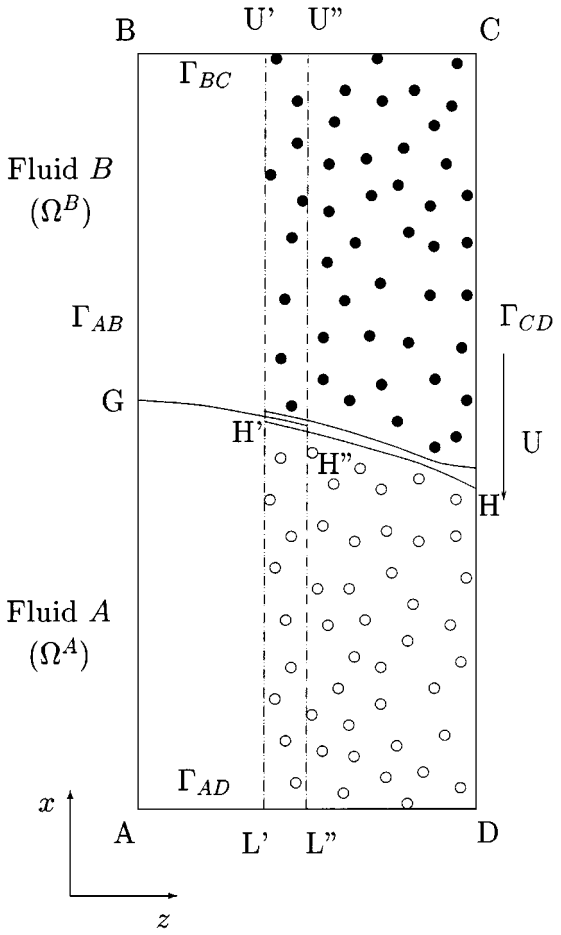

FIG. 2. Hybrid formulation geometry showing the molecular region boundary $\Gamma_{\text{mol}} = \text{L}'\text{U}'$ and the continuum region boundary $\Gamma_{\text{cont}} = \text{L}''\text{U}''$.

complex and requires the ability to simulate flows with a component normal to the interface between the two subdomains (molecular and continuum). The results of our hybrid solution technique are compared to a fully molecular solution on the same geometry which is taken to be the exact solution. The computational domain size is small enough so that it can be treated by molecular dynamics in its entirety. As a result the hybrid geometry involves continuum regions that are of size comparable to the molecular regions, and thus no real computational gain is obtained.

2.2. *Molecular Dynamics Simulations*

We describe here the MD simulation of the immiscible fluid displacement problem. The channel geometry (length L and width $2H$) is shown in Fig. 3. Note that in the molecular simulations the symmetry about the channel centerline is utilized in a different way compared to continuum techniques because symmetry boundary conditions are difficult to impose in MD simulations. The simulation domain covers the full channel width and the extra simulation cost is offset by the number of statistical data obtained. Additionally, again

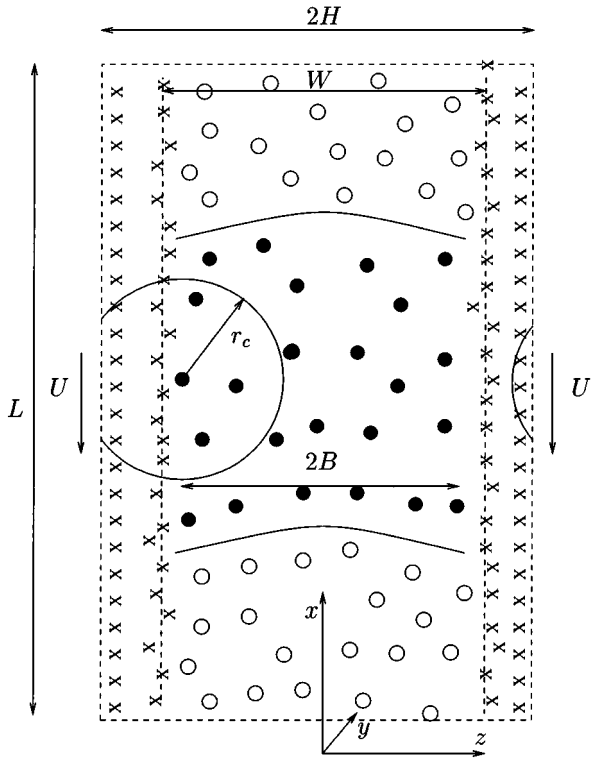

FIG. 3. Problem geometry for the MD simulation. r_c is the interaction cutoff length. Wall molecules are denoted by $\times$, fluid A molecules by open circles, and fluid B molecules by solid circles (not to correct density for clarity).

for reasons of computational convenience, periodic boundary conditions are applied in the streamwise direction, which is allowable because of the interchangeability of fluids A and B.

Unless otherwise stated, all quantities will be expressed in reduced units using $\sigma = \sigma_{\mathrm{Ar}} = 3.4$ Å for length, $m = m_{\mathrm{Ar}} = 40$ amu for mass, $\varepsilon/k_{\mathrm{b}} = \varepsilon_{\mathrm{Ar}}/k_{\mathrm{b}} = 119.8^{\circ}$K for temperature, and $\tau = (m\sigma^2/48\varepsilon)^{1/2} = 3.112 \times 10^{-13}$ s for time. Here k_{b} is Boltzmann's constant, σ_{Ar} and $\varepsilon_{\mathrm{Ar}}$ are the parameters of the Lennard–Jones (LJ) potential for argon [15], m_{Ar} is the mass of the argon atom, and τ is the characteristic time for argon. The interaction potential was truncated at the rather conservative cutoff length $r_{\mathrm{c}} = 3\sigma$. The simulation box is a fully periodic MD domain of size $(L \times D \times W) = (57.05\sigma \times 5.56\sigma \times 15.29\sigma)$ in the x, y, and z directions, respectively.

The molecular model for the two fluids is the same as in [9, 14]; the argon molecules are divided into two subspecies: subspecies A and B. These two subspecies (1280 molecules each) are completely identical because they have the same self-interactions and interactions with the walls of the system; they are, however, immiscible because the potential interaction between them is repulsive. More specifically, the potential used in this study,

$$V_{ij}(r) = 4\varepsilon_{ij}\left[(\sigma_{ij}/r)^{12} - \delta(\sigma_{ij}/r)^{6}\right], \tag{1}$$

where r is the separation of the two interacting molecules, is a modified [9] form of the well-known Lennard–Jones potential ($\delta = 1$). For the interaction between subspecies A and B, $\delta = -1$; for all other pairs of interactions $\delta = 1$.

The above fluid characteristics were "constructed" for reasons of computational simplicity but also ease of matching of the molecular system properties with the continuum system properties. In continuum terms the behavior of the above molecular system is equivalent to that of two fluids with the same density and viscosity (equal to bulk values for liquid argon); the fluids, however, are immiscible with a surface tension coefficient γ which can be calculated from molecular techniques: at the temperature ($T = 1.4$) and density ($\rho = 0.81\sigma^{-3}$) of the simulation, $\gamma = 3.9 \pm 0.2\varepsilon/\sigma^2$ [14]. More importantly, the two fluids interact with the two bounding walls in exactly the same way, and therefore the static contact angle, by symmetry arguments, has to equal 90°.

The fairly repulsive potential interaction between the two fluids results in a gap of the order of 1σ between the two fluids. More realistic potentials, or alternatively the simulation of a fluid and its vapor, would result in significantly more diffuse interfaces that would require modeling assumptions for the exact definition of their locations. We thus preferred this slightly artificial interaction which we believe does not affect the generality of our conclusions since the surface tension associated with it can be calculated.

Each of the two parallel, isothermal walls bounding the fluids is modeled by 600 wall molecules arranged in an *fcc* two-layer structure in the x–y plane. The wall density, ρ_w, is equal to the fluid density, ρ. The outer of the two layers is constrained to move with velocity $-U$ in the x direction and the molecules composing it do not have thermal velocities. The inner layer obeys the usual Newtonian equations of motion but its temperature is rescaled in order for it to act as an energy sink and allow the simulation to reach a steady nonequilibrium state by effectively imposing temperature boundary conditions on the fluid argon. Similar models have been shown [13] to adequately capture the dynamics of wall–fluid interactions. The combined thickness (along the z direction) of the two walls is greater than the interaction potential cutoff (r_c) such that

$$2H - W > r_c,$$

and thus the fluid molecules do not see their images across the walls (see Fig. 3). The wall (W) and wall–fluid (WF) potential parameters are $m_W = 2m_{Ar}$, $\varepsilon_W = 5\varepsilon_{Ar}$, $\sigma_W = \sigma_{Ar}$, $\varepsilon_{WF} = 1.03\varepsilon_{Ar}$, and $\sigma_{WF} = 1.03\sigma_{Ar}$. They do not represent any known solid material. They were chosen as a good compromise between the requirements of minimum number of wall molecules, a melting point that exceeds the highest temperature encountered during the simulation, minimum layering of the argon molecules close to the walls, and minimum slip length. The width of the channel (H) is determined by the average location of the first layer of wall molecules (Fig. 3). However, the volume occupied by the fluid is less due to the finite repulsive core of the interaction potential between the walls and the fluid. We denote the thickness of the "fluid region" by $2B$, where $H = 1.16B$.

After an equilibration period of 640τ, samples are taken for a further 2720τ. The flow field is recovered by averaging the instantaneous molecular velocities in rectangular bins spanning the x–z plane. The size of the bins is 1.43σ along the x direction and 1.53σ along the z direction. The resulting statistical errors for the velocity are expected to be less than $0.002\sigma/\tau$.

The flow field (Fig. 4) is generated by forcing the fluid into the Poiseuille parabolic profile far away from the two-fluid interface. We have ensured that the distance between the two two-fluid interfaces is greater than $5H(L > 10H)$, such that the assumption of a Poiseuille profile is valid; various studies [16, 17] have verified that the flow field relaxes to

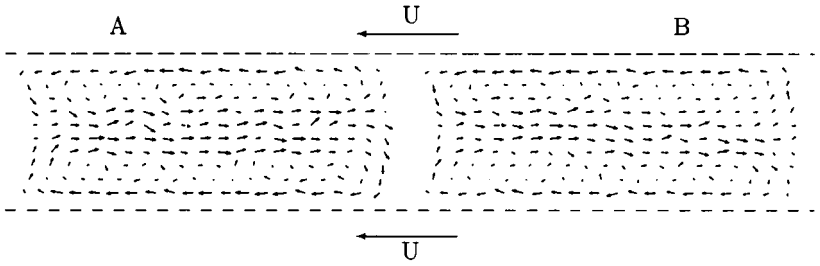

FIG. 4. Flow field for Poiseuille configuration. Both walls move with velocity $-U = -0.017\sigma/\tau$.

the above profile at distances greater than $2.5H$ from the interface. The Poiseuille profile is a zero-mass-flux profile because the simulation takes place in the reference frame of the moving interface. The velocity profile was imposed through the method developed in [6] and is discussed in Section 2.2.1.

Due to the periodic boundary conditions in the streamwise direction there are two two-fluid interfaces; in one, fluid A advances into fluid B and in the other, fluid B advances into fluid A. Because the gap between the two fluids is not constant but varies as a function of z, we defined each two-fluid interface using two lines: each line represents the envelope of the average extreme excursions of one fluid in the streamwise direction. For example, at the interface where fluid A is advancing into fluid B, one line represents the mean maximum excursion of fluid A and the other line represents the mean minimum excursion of fluid B. In Fig. 5 we retain both lines to indicate the molecular interface shape, but we reduce their gap at the centerline of the channel to zero, to facilitate comparison of both their relative curvatures as well as with the continuum results. Note that the two lines diverge close to

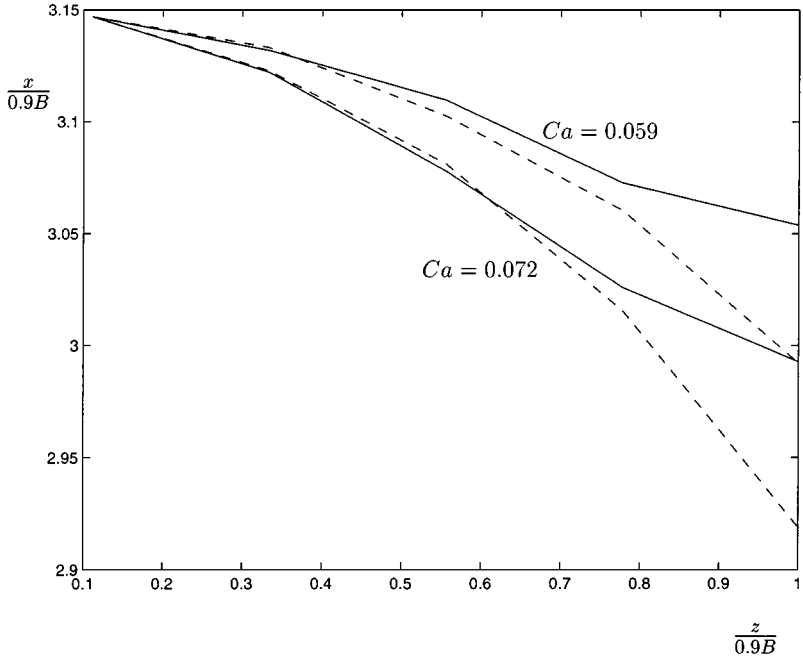

FIG. 5. The two-fluid interface shapes for different Ca. Advancing fluid fronts are shown as solid lines and receding fluid fronts as dashed lines. The channel centerline is at $z = 0$.

the wall, indicating that the accommodation of the shearing from the wall requires the gap between the two fluids to increase. This is clearly a molecular phenomenon that cannot be captured by a continuum simulation.

2.2.1. Boundary Condition Imposition. The imposition of boundary conditions on MD simulations is essential to the success of a hybrid technique. Although boundary conditions are only required on Γ_{mol} in the hybrid case, we used our boundary condition imposition technique for forcing the parabolic velocity profile in the streamwise direction for both the fully molecular and the hybrid computations. In the case of the fully molecular solution, we ensured that the flow field is consistent with previous reports of similar work, by comparing the results of the above method with results obtained using gravity as the driving force for the fluid motion [13]. We also performed "in-house" comparisons using gravity as the driving force for the flow: the results of the two simulation methods for the same wall velocity (U) are indistinguishable within the statistical accuracy of the simulations [18].

In the case of the imposition of the Poiseuille profile across the channel width the technique utilizes thin (thickness $\Delta \sim 1\sigma$) regions, denoted momentum reservoirs (Fig. 6), surrounding the Dirichlet boundaries in which the velocity of the molecule is set to the

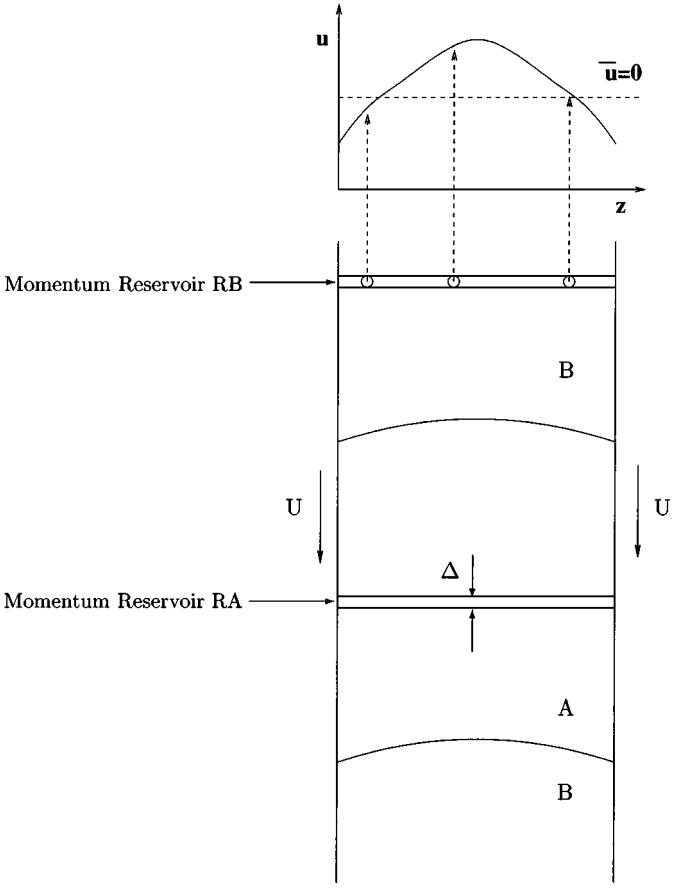

FIG. 6. Flow field imposition method. Particles in reservoirs RA and RB of thickness Δ are forced to a velocity boundary condition $u = \mathbf{v}_{\text{bc}}$ depending on their position z. The average $\bar{u}$ is equal to zero (no net mass flux) in this particular problem.

requisite boundary condition through the use of biased Maxwellian distributions [18]

$$f(\mathbf{v}) = \left(\frac{\mathrm{m}}{2\pi k_\mathrm{b} T_\mathrm{bc}(\mathbf{x})}\right)^{3/2} \exp\left(-\frac{(\mathbf{v}-\mathbf{v}_\mathrm{bc}(\mathbf{x}))^2}{2k_\mathrm{b} T_\mathrm{bc}(\mathbf{x})}\right). \tag{2}$$

Here $\mathbf{v}_\mathrm{bc}(\mathbf{x})$ is the requisite velocity boundary condition, $T_\mathrm{bc}(\mathbf{x})$ is the requisite temperature boundary condition. These regions have a finite thickness, so that the boundary condition imposition provides information about the local field variable gradients in addition to the information about the local field variables; this addition partially offsets the error associated with the use of the approximate Maxwellian distribution due to the incomplete knowledge of the dense fluid non-equilibrium distribution function. The use of the dense hard sphere Enskog correction [19] is under investigation.

The technique also requires regions called particle reservoirs through which the fluid can flow to and from the various boundary regions such that the correct feed of molecules is supplied to the simulation region in order for mass conservation to be honored. Any closed (or periodic) extension (for dicussion of limitations see [18]) of the simulation domain can serve as a particle reservoir.

The periodicity of the solution renders the particle reservoirs unnecessary. This is better illustrated in Fig. 6: the complete domain can be seen as two simulation domains (as described in Fig. 2) joined back to back, taking advantage of the interchangeability of fluid A and B to dispense with the particle reservoir. Momentum reservoir RA, for example, induces inflow to the top half of the simulation, but also outflow to the bottom half of the simulation; subsequently, each simulation half can be viewed as the particle reservoir of the complementary remaining half.

2.3. *The Finite Element Technique*

The continuum part of the hybrid solution comes from an isoparametric finite element discretization of the Stokes equations [16]

$$\frac{\partial \tau_{ij}}{\partial x_j} = 0, \tag{3}$$

$$\frac{\partial u_i}{\partial x_i} = 0, \tag{4}$$

which are the appropriate low-speed ($\mathrm{ReCa} \ll 1$, $\mathrm{Re} = \rho U H/\mu$) limits of the governing Navier–Stokes equations [21]. Here τ_{ij} is the stress tensor and $i = 1, 2, 3$ corresponds to directions x, y, and z, respectively. The simulation was performed in the Stokes limit since the Weber number ($\mathrm{We} = \mathrm{ReCa} = \rho U^2 H/\gamma$) that measures the effect of the inertia forces with respect to the capillary forces was always less than 0.02. Previous work [20, 21], both analytical and computational, indicates that for a Weber number of 0.01 the error in neglecting the inertial terms is less than 1%. Recall that the error associated with the MD procedure is estimated to be 5–10%.

The solution of this problem is challenging because the two-fluid interface shape couples non-linearly to the flow field through the following stress balance:

$$\hat{n}_i\left(\tau_{ij}|_{\Gamma_\mathrm{f}^\mathrm{B}} - \tau_{ij}|_{\Gamma_\mathrm{f}^\mathrm{A}}\right)\hat{n}_j = \gamma\kappa \qquad \text{on } \Gamma_f, \tag{5}$$

$$\hat{t}_i\left(\tau_{ij}|_{\Gamma_\mathrm{f}^\mathrm{B}} - \tau_{ij}|_{\Gamma_\mathrm{f}^\mathrm{A}}\right)\hat{n}_j = 0 \qquad \text{on } \Gamma_f. \tag{6}$$

Here $\hat{n}_i$ and $\hat{t}_i$ are the right-handed outward unit normal and tangent on the interface Γ_f, $\Gamma_f^B = \Gamma_f \cap \Omega^B$ and $\Gamma_f^A = \Gamma_f \cap \Omega^A$, and κ is the curvature. The variational form of this boundary condition, obtained by Ruschak [22], has been used here to obtain a variationally consistent finite element approximation.

The remaining boundary conditions are

$$\frac{dx_s(0)}{ds} = 0, \tag{7}$$

$$\frac{dx_s(S)}{ds} = \cos\theta \tag{8}$$

for the contact angle and

$$u_z = 0 \qquad \text{on } \Gamma_{AB}, \Gamma_{AL''}, \Gamma_{BU''} \tag{9}$$

$$u_x = Ug, \qquad \text{on } \Gamma_{AL''}, \Gamma_{BU''}, \tag{10}$$

$$\sigma_{xz} = 0 \qquad \text{on } \Gamma_{AB}, \tag{11}$$

$$u_x = (u_{MD})_x, \qquad \text{on } \Gamma_{cont} \tag{12}$$

$$u_z = (u_{MD})_z, \qquad \text{on } \Gamma_{cont} \tag{13}$$

for the flow field. Here s is the arc length coordinate along Γ_f such that $s = 0$ and $s = S$ correspond to points G and H″ on Γ_f, respectively; Γ is the union of Γ_{AB}, $\Gamma_{BU''}$, $\Gamma_{U''L''}$, and $\Gamma_{AL''}$; $x_s(z)$ is the two-fluid interface position as a function of z; u_{MD} is the Dirichlet data from the molecular dynamics simulation; and g is the parabolic zero-mass-flux profile, $g(\frac{z}{H}) = \frac{1}{2} - \frac{3}{2}(\frac{z}{H})^2$.

An algorithm that makes use of the importance of surface tension for $\mathrm{Ca} < 0.1$ to converge rapidly to the steady-state solution [18] was also developed. The algorithm is based on a modified form of Eq. (5),

$$\hat{n}_i\left(\tau_{ij}|_{\Gamma_f^B} - \tau_{ij}|_{\Gamma_f^A}\right)\hat{n}_j - \gamma\kappa = \gamma\kappa(\Delta x) \qquad \text{on } \Gamma_f, \tag{14}$$

where $\kappa(\Delta x)$ is the curvature correction required to balance (5). This equation takes advantage of the fact that only the correct steady-state solution can satisfy both conditions required at the interface, namely (5) which is the normal momentum balance, and

$$\hat{n}_i u_i = 0, \tag{15}$$

which is also known as the kinematic condition.

Based on this observation [16], the following iterative procedure can be applied: (i) a guess interface shape is assumed; (ii) the Stokes problem subject to the boundary conditions given above and the kinematic condition on the fixed interface shape provides a flow field solution; (iii) the residual of (5) gives a correction displacement ($\Delta x(z)$) by solving (14); and (iv) the interface is updated to the new shape based on the correction displacement $\Delta x(z)$. Steps (ii)–(iv) are repeated to convergence. For $\mathrm{Ca} < 0.1$ this procedure converges to the correct solution in less than five iterations. The full details of the algorithm, the solvability issues resulting from the application of the kinematic condition, and the variational formulations can be found in [18].

The continuum solver requires an angle boundary condition for the point where the two-fluid interface meets Γ_{cont} (point H″); it, of course, requires one at point G which is always 90° by symmetry. The angle boundary conditions are of the natural form, and are a result of the weak formulation of the governing equations [18]. The angle at point H″ is evaluated by averaging the shape of the interface in the molecular solution and extracting its slope at H″.

The discretization uses an isoparametric finite element solver with a structured mesh that is refined to mesh sizes at least one order of magnitude smaller than the slip length close to point H″ for complete resolution of the angle imposition. We have used the Crouzeix–Raviart elements, which can correctly capture the pressure discontinuity at the two-fluid interface because they allow pressure discontinuities across element edges. More details on the finite element methodology can be found in [18].

3. HYBRID SOLUTION

3.1. *Formulation*

In the hybrid solution presented in this section we use the ingredients presented in Sections 2.2 and 2.3; namely, we use MD to describe region L′U′CD and continuum fluid mechanics (finite elements) to describe region ABU″L″. We compare this solution to the fully molecular solution of Section 2.2.

The channel dimensions favored the extension of the molecular region to the full channel length (up to Γ_{BC} and Γ_{AD}); slip was important in approximately 50% of the channel length which was large enough to make the addition of a continuum region in the streamwise direction impracticable. This, of course, will not be the case for macroscopic problems in which slip is limited to very small fractions of the channel length.

Our approach to this problem is an extension of the Schwarz technique presented in [6] and Section 1.2: the continuum solution from the previous iteration provides new boundary conditions for the molecular simulation on the boundary of the latter ($L'U' \equiv \Gamma_{mol}$), which lies well within the continuum domain (thickness of the overlap region $= 0.2B$); the new molecular solution in turn provides a new set of boundary conditions for the continuum simulation on the boundary of the latter ($L''U'' \equiv \Gamma_{cont}$), which lies inside the molecular domain. This completes one full iteration. Figure 7 shows the molecular data on Γ_{cont} which serve as boundary conditions for the continuum simulation. Because of the statistical nature of the MD data the velocity profiles are smoothed before being passed to the continuum simulation. The smoothing is achieved through a low-order (fifth-order) fit. The simulation is isothermal and hence the energy equation is not considered in the continuum domain; the boundary data exchanged are limited to flow velocities and the angle of the interface at H″ which enters the continuum calculation as a natural boundary condition [18]. The molecular calculation does not require angle information. Convergence obtains when the two solutions are identical throughout the overlap region.

The velocity boundary conditions in the MD simulations are imposed on Γ_{mol}, $\Gamma_{U'C}$, and $\Gamma_{L'D}$ using momentum reservoirs discussed in Section 2.2.1. Region ABU′L′ is used as a particle reservoir [18]; that is, during the molecular simulations it is part of the simulation domain although the solution in this region is now a complement of the molecular solution of interest in region L′U′CD. Region ABU′L′ ensures that the right number of molecules of type A are injected into region L′H′HD through face L′H′ to satisfy the inflow boundary condition

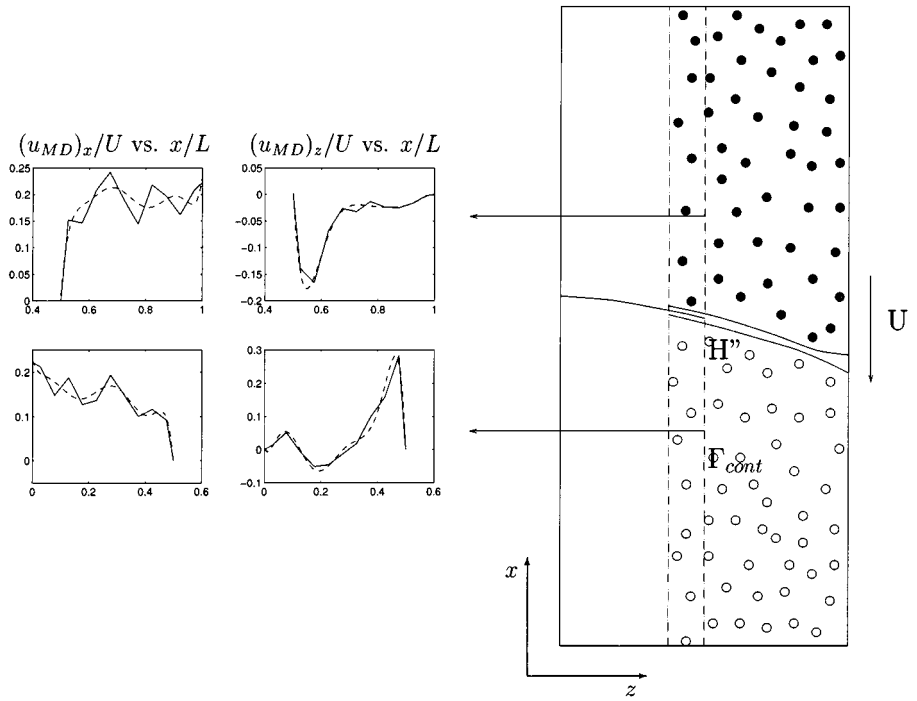

FIG. 7. Molecular data on Γ_{cont} is used as boundary conditions for the continuum simulation. The solid line represents the actual data, and the dashed line, the fit used to impose the data. Angle information at point H″ is also used.

on this face, and similarly the right number of molecules of type B are absorbed from region H′U′CH to satisfy the outflow boundary condition on face H′U′. To prove this, recall that in steady elliptic incompressible problems (where the Mach number is negligibly small compared to 1) the net mass flux through any closed region is zero. The imposition of zero-net-mass-flux boundary conditions thus forces the correct "particle feed flow field" in the particle reservoirs with inflow/outflow regions in contact with the respective outflow/inflow regions of the simulation region, since the individual net mass flux both of the reservoir regions and of the simulation region is zero. In the above example the flux through face H′U′ absorbed by the particle region is balanced (to achieve zero net mass flux) by the outflow through face BU′; a close examination of the flow field in Fig. 4 indicates that the outflow through face BU′ returns (due to the periodicity of the solution) to the simulation region through face U′C to complete the no-net-mass-flux requirement for the simulation region.

The normal velocity profiles were corrected for mass continuity before being passed to the continuum domain by requiring that the net mass flux of each fluid through the continuum domain equals zero. For example, for fluid A we require

$$\left(u_{\text{MD}}^{\text{L}''\text{H}''}\right)_z = \left(u_{\text{MD}}^{\text{L}''\text{H}''}\right)_z - \frac{\int_{\text{L}''\text{H}''} \left(u_{\text{MD}}^{\text{L}''\text{H}''}\right)_z \, dl - \int_{\text{AL}''} Ug \, dl}{\int_{\text{AL}''} dl}. \tag{16}$$

As in Section 2.3, $(u_{\text{MD}})_z$ denotes the normal boundary data from the molecular dynamics simulation on the portion of Γ_{cont} indicated, and Ug denotes the zero-net-mass-flux boundary condition on sections Γ_{BC} and Γ_{AD}.

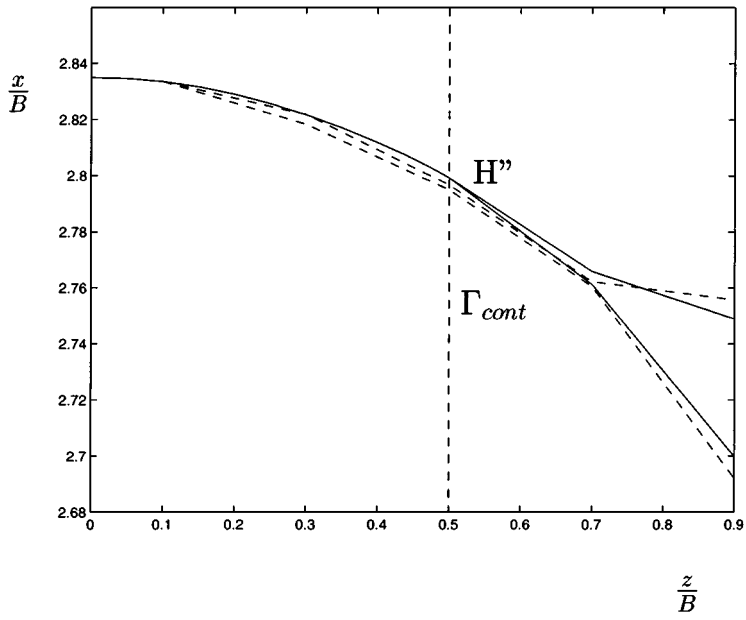

FIG. 8. Comparison of the fully molecular (dashed) and hybrid (solid) interface shape for $\mathrm{Ca} = 0.059$.

3.2. *Results*

We now present the results of the hybrid formulation for a capillary number of $\mathrm{Ca} = 0.059$. In this problem we have chosen the fully continuum solution for $\mathrm{Ca} = 0.059$ presented in Fig. 5 as the initial guess solution. This choice significantly reduces the computational effort required since the starting solution is close to the exact (fully molecular) solution and therefore a few iterations will suffice to obtain complete convergence. The issue of convergence of the modified Schwarz technique from initial guess solutions arbitrarily far from the exact solution is left as the subject of future work.

Figure 8 shows the results obtained after two iterations. We can see that the results are in very good agreement with the corresponding fully molecular results. Note that the hybrid interface shape consists of a single line in the continuum subdomain up to point H″ and two lines in the molecular domain. The molecular solution and the molecular part of the hybrid solution consist of two lines as discussed in Section 2.2.

4. EFFICIENCY CONSIDERATIONS

The computational work associated with a hybrid solution can, to a very good approximation, be attributed to the molecular part; for each iteration the continuum iterate typically takes two orders of magnitude less computational time than the molecular iterate. In what follows we will neglect the computational cost of the continuum solutions in order to simplify our investigation, which aims at minimizing the computational cost of the complete hybrid solution.

Convergence can be proven for a large class of problems when both subdomains are treated by continuum methods [11]. In particular, elliptic problems, such as those treated in this paper, are amenable to analysis which yields useful results: convergence exhibits a

power law behavior of the form

$$\varepsilon^{n+1} = K\varepsilon^n, \tag{17}$$

where K is a positive constant ($0 < K < 1$) which governs the convergence rate and ε is the error in the appropriate norm [11] and n is the iteration number. The constant K depends on the particular problem at hand through the governing operator eigenvalues [11], but also on the size of the overlap region: the larger the overlap region, the smaller K is, and hence the faster the convergence.

Convergence should also be obtained for a hybrid description if the continuum and molecular models are equivalent in the overlap region. However, additional "steady-state" errors will arise in the hybrid case due to, first, discrepancies in the transport coefficients in the two subdomains, second, noise introduced by MD statistical fluctuations, and third, smoothing of the MD data prior to imposition of the boundary conditions on the continuum iterate. The convergence *rate* may also be affected by these new sources of error.

If we neglect the continuum cost of the solution we can easily express the total cost (or work W) of the hybrid solution as

$$W = \text{work per MD time step} \sum_{i=1}^{n_0} N_i, \tag{18}$$

where n_0 is the total number of iterations and N_i is the number of molecular dynamics time steps run at iteration i. The expected error in a field quantity from the MD iterate i is given by

$$\epsilon_i = \frac{A}{\sqrt{N_i}}, \tag{19}$$

where A is a constant (for a given simulation) that can easily be estimated [15, 18]. We would like to know how the error in the initial stages of the iteration propagates, accumulates, and affects the final error present at convergence; if the effect of the error decays sufficiently fast we can design a "schedule" for the number of MD time steps as a function of the iteration number such that initial MD simulations are run to low accuracy, thus reducing the computational cost.

Under the above assumption of Gaussian statistics we model the convergence procedure as a stochastically forced decay process leading to a governing equation [18]

$$\varepsilon^{n+1} = K\varepsilon^n + \epsilon^n, \tag{20}$$

which has the general solution

$$\varepsilon^n = \sum_{j=0}^{n-1} K^{n-1-j}\epsilon^j + K^n\varepsilon^0. \tag{21}$$

We will now look for the error behavior as a function of the iteration number. We introduce statistics in an ensemble sense, that is,

$$\overline{\varepsilon^n} = \lim_{M\to\infty} \frac{1}{M} \sum_{k=1}^{M} \varepsilon_k^n, \tag{22}$$

and

$$\mathrm{Var}(\varepsilon^n) = \lim_{M\to\infty} \frac{1}{M} \sum_{k=1}^{M} \left(\varepsilon_k^n - \overline{\varepsilon^n}\right)^2, \tag{23}$$

where $k = 1, \ldots, M \to \infty$ are the different realizations of similar systems characterized by (20). Using

$$\overline{\epsilon^n} = \lim_{M\to\infty} \frac{1}{M} \sum_{k=1}^{M} \epsilon_k^n = 0 \qquad \forall n, \tag{24}$$

$$\mathrm{Var}(\epsilon^n) = \lim_{M\to\infty} \frac{1}{M} \sum_{k=1}^{M} \left(\epsilon_k^n\right)^2 = \frac{A^2}{N_n}, \tag{25}$$

and

$$\mathrm{Var}(\varepsilon^0) = 0, \tag{26}$$

it can easily be shown that

$$\mathrm{Var}(\varepsilon^{n_0}) = \sum_{j=0}^{n_0-1} K^{2(n-1-j)} \mathrm{Var}(\epsilon^j) = \sum_{j=0}^{n_0-1} K^{2(n-1-j)} \frac{A^2}{N_j}. \tag{27}$$

Also note that we have assumed that the cross-correlation terms in the ensemble sense ($\lim_{M\to\infty} \frac{1}{M} \sum_{k=1}^{M} \epsilon_k^n \epsilon_{k+j}^n$, $j \neq 0$) go to zero.

We have verified the validity of the above equations with numerical simulations. An ensemble of 1000 members all obeying the difference equation (20) was simulated using a Gaussian generator to model the stochastic error term. The results (see [18]) verify the correctness of the equations derived above: the mean value of the error decays as in the unforced case, and the expected error (associated with one standard deviation) is given by (27).

We therefore seek the optimal scheduling of the number of molecular dynamics time steps as a function of the iteration number (n), by also allowing the total number of iterations (n_0) to vary, subject to the constraint of a desired simulation accuracy. We can pose the constraint as

$$K^{n_0}\varepsilon^0 + \sigma(\varepsilon^{n_0}) = B, \tag{28}$$

where in doing so, we have associated one standard deviation of the stochastic part of ε^{n_0} to the expected error and added that to the error at the n_0 iteration due to the deterministic part ($K^{n_0}\varepsilon^0$), and required that it equal B.

We form the Lagrangian

$$\mathcal{L} = \sum_{j=1}^{n_0} N_j + \lambda \left(K^{n_0}\varepsilon^0 + \sqrt{\sum_{j=0}^{n_0-1} K^{2(n-1-j)} \frac{A^2}{N_j}} - B \right) \tag{29}$$

which can be differentiated for the determination of the extrema. These are obtained for

$$N_j = \frac{A^2}{(B - K^{n_0}\varepsilon^0)^2} \frac{K^{-1} - K^{n_0-1}}{K^{-1} - 1} K^{n_0-1-j}, \tag{30}$$

that is, for a given n_0 the optimum work is achieved for $N_j \propto K^{n_0-1-j}$.

We will now seek the optimum n_0 by substituting the expression we have found for N_j into (18) and finding for which n_0 a minimum is obtained. The expression for the cost is

$$W = \frac{A^2}{(B - K^{n_0}\varepsilon^0)^2}\left(\frac{K^{-1} - K^{n_0-1}}{K^{-1} - 1}\right)^2. \tag{31}$$

Note that this expression is singular for $B = K^{n_0}\varepsilon^0$ because an infinite number of time steps are required for the stochastic term to go to zero such that B is balanced only by the initial condition decay term. We can look for minima for $n_0 > \ln B/\ln K$ ($\varepsilon^0 = 1$) because the branch $n_0 < \ln B/\ln K$ corresponds to the negative value of the square root in (29) and represents the case for which $(B - K^{n_0}\varepsilon^0) < 0$. For $n_0 > \ln B/\ln K$, W is monotonically decreasing and this indicates that the optimum is obtained for $n_0 \to \infty$.

Since an infinite number of iterations is impossible, we show here that this infinity can be replaced by a suitably large number with a very small effect on the work savings. We illustrate this with a numerical example: using $B = 0.3$, $\varepsilon^0 = 1$, $K = 0.1$, and $A = 1$ we need $n_0 = 25$ for $\sigma = \text{const.} = 0.1$. This translates to a total work of $W = 2500$ (in arbitrary units). Using the scheme derived above (30) with $n_0 = 81$ we find that the error decays to the target value of 0.3, but the work is now $W = 1112.1$. Additionally we can use (31) to find $W(n_0 \to \infty) = 1111.1$ which shows that less than 0.1% is lost by taking $n_0 = 81$, but also that a factor of 2.5 in savings is obtained through the use of the optimal scheduling technique. Figure 9 shows numerical results obtained by a stochastic simulation; the results verify the theoretical predictions of (30). The work was also evaluated directly

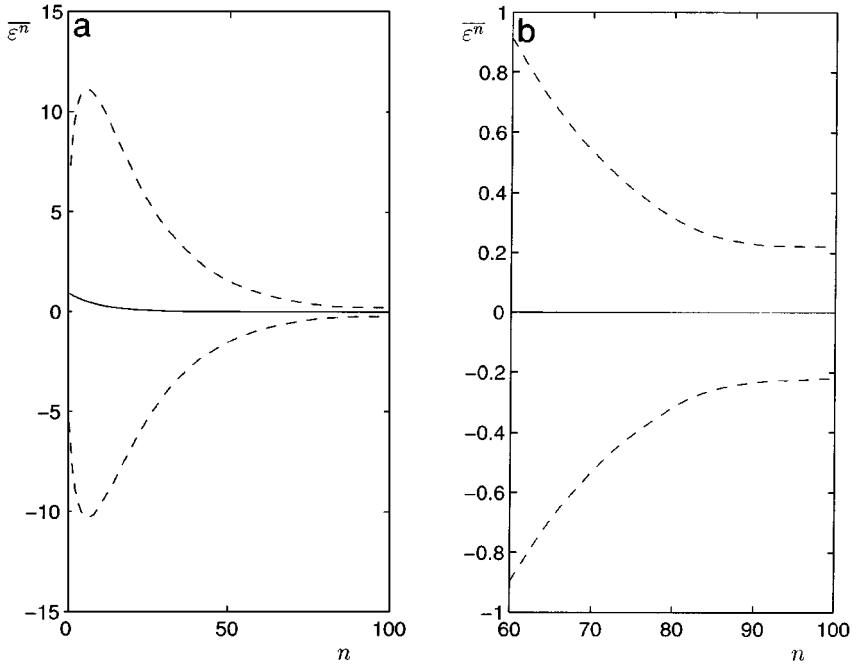

FIG. 9. Numerical simulation of (20) subject to the scheduling of (30) with $B = 0.3$, $\varepsilon^0 = 1$, $K = 0.1$, $A = 1$, and $n_0 = 81$. The results are ensemble (1000 members) averaged and n is the iteration number. The solid line shows that $\overline{\varepsilon^n}$ decays like the unforced case, whereas the dashed lines show $\overline{\varepsilon^n} \pm \sigma(\varepsilon^n)$. Panel (a) shows the full results ($n = 0$–100), and Panel (b) focuses ($n = 60$–100) on the crossover ($B = K^{n_0}\varepsilon^0 + \sigma(\varepsilon^{n_0})$) at $n = n_0 = 81$.

from the stochastic simulation and found to equal the theoretical value of $W = 1112.1$. Further numerical experiments indicate that as $B \to 0$ this scheduling technique becomes more effective with gains exceeding the value of 3.

5. CONCLUDING REMARKS

From the results of Section 3 we can conclude that the hybrid technique developed can capture the dynamics of complex multi-fluid fluid mechanical phenomena. Our current results indicate that the modified Schwarz method for two fluids converges from initial conditions close to the final result. Future work includes further simulations to establish the (expected) unconditional convergence of the iteration from arbitrary initial interface shapes.

Additional work is required for the development of a more accurate boundary condition imposition technique as this ultimately limits the accuracy of the results of a hybrid simulation. In one-dimensional problems it can be shown [18] that the error due to the boundary condition imposition is suppressed by a factor monotonically increasing with the width of the overlap region. Unfortunately no such result exists for the two-dimensional case, and the results of [6] suggest that the boundary condition error might be amplified and result in inaccurate hybrid solutions. In this work the presence of the full channel minimizes the error in the final solution; despite this further work is required to reduce the error in imposing general boundary conditions in MD simulations.

Figure 7 shows that the molecular velocity data are appreciably noisy. The solution for the interface shape is fairly insensitive to this noise, as the good agreement of the hybrid result with the fully molecular solution indicates. There may be, however, classes of problems that are not so insensitive and hence, more attention needs to be paid to the effect of the statistical nature of MD to hybrid solution frameworks. As discussed in Section 4, because of the statistical nature of MD the convergence of the iteration procedure needs to be examined in a statistical framework. The accuracy and the convergence rate of the hybrid solution may be adversely affected; the use of an elementary smoothing technique (low-order fit) has been shown to work fairly effectively but its full effect is not completely understood.

The simulation presented in this work was at the molecular scale; the continuum domain was of the same size (approximately) as the molecular domain. This approach was preferred over a solution where the continuum domain would be substatially larger than the molecular domain because at this stage we were interested in a direct comparison between the hybrid solution and the fully molecular solution that yields important information about the accuracy of the hybrid technique. In fact, the molecular model used here has no real-world analogue and hence no meaningful comparison to any macroscopic solution or experimental data can be expected. Additionally, the extension to macroscopic problems presents no additional challenges, but rather some improvements of the current technique that can be reasonably easily effected. A full macroscopic simulation is currently under investigation.

ACKNOWLEDGMENTS

This work was supported by DARPA and the ONR under Grant N00014-91-J-1889. The author thanks Anthony T. Patera, his thesis advisor, for helpful comments, suggestions, and discussions, and Berni J. Alder for critically commenting on the manuscript.

REFERENCES

1. S. Kohlhoff, P. Gumbsch, and H. F. Fischmeister, Crack propagation in b.c.c. crystals studied with a combined finite-element and atomistic model, *Philos. Mag. A* **64**, 851 (1991).
2. D. C. Wadsworth and D. A. Erwin, One-dimensional hybrid continuum/particle simulation approach for rarefied hypersonic flows, AIAA Paper 90-1690 (1990).
3. J. F. Bourgat, P. Le Tallec, D. Tidriri, and Y. Qiu, Numerical coupling of nonconservative or kinetic models with the conservative compressible Navier–Stokes equations, in *Fifth International Symposium on Domain Decomposition Methods for Partial Differential Equations*, edited by R. Glowinski, G. Meurant, B. Voigt, and O. Widlund (SIAM, Philadelphia, 1991), p. 420.
4. D. B. Hash and H. A. Hassan, A hybrid DSMC/Navier–Stokes solver, AIAA Paper 95-0410 (1995).
5. S. T. O'Connell and P. A. Thompson, Molecular dynamics–continuum hybrid computations: A tool for studying complex fluid flows, *Phys. Rev. E* **52**, (1995).
6. N. Hadjiconstantinou and A. T. Patera, Heterogeneous atomistic–continuum representations for dense fluid systems, *Int. J. Modern Phys. C* **8**, 967 (1997).
7. A. L. Garcia, J. B. Bell, W. Y. Crutchfield, and B. J. Alder, Adaptive mesh and algorithm refinement using direct simulation Monte Carlo, *J. Comp. Phys.*, to appear.
8. E. B. Dussan, On the spreading of liquids on solid surfaces: Static and dynamic contact angles, *Annu. Rev. Fluid Mech.* **11**, 371 (1979).
9. P. A. Thompson and M. O. Robbins, Simulations of contact-line motion: Slip and the dynamic contact angle, *Phys. Rev. Lett.* **63**, 766 (1989).
10. N. Hadjiconstantinou, Combining atomistic and continuum simulations of contact line motion, *Phys. Rev. E* **59**, 2475 (1999).
11. P. L. Lions, On the Schwarz alternating method, I, in *First International Symposium on Domain Decomposition Methods for Partial Differential Equations*, edited by R. Glowinski, G. Golub, G. Meurant, and J. Periaux (SIAM, Philadelphia, 1988), p. 1.
12. J. Koplik and J. R. Banavar, Continuum deductions from molecular hydrodynamics, *Annu. Rev. Fluid Mech.* **27**, 257 (1995).
13. J. Koplik, J. R. Banavar, and J. F. Willemsen, Molecular dynamics of fluid flow at solid surfaces, *Phys. Fluids A* **1**, 781 (1989).
14. P. A. Thompson, W. B. Brinckerhoff, and M. O. Robbins, Microscopic studies of static and dynamic contact angles, *J. Adhesion Sci. Technol.* **7**, 535 (1993).
15. M. P. Allen and D. J. Tildesley, *Computer Simulation of Liquids* (Oxford Univ. Press, Oxford, 1987).
16. J. Lowndes, The numerical simulation of the steady movement of a fluid meniscus in a capillary tube, *J. Fluid Mech.* **101**, 631 (1980).
17. I. B. Bazhlekov and A. K. Chesters, Numerical investigation of the dynamic influence of the contact line region on the macroscopic meniscus shape, *J. Fluid Mech.* **329**, 137 (1996).
18. N. Hadjiconstantinou, *Hybrid Atomistic–Continuum Formulations and the Moving Contact Line Problem*, Ph.D. thesis (Mechanical Engineering Department, MIT, 1998).
19. J. O. Hirschfelder, C. F. Curtiss, and R. B. Bird, *Molecular Theory of Gases and Liquids*, Wiley, New York, 1964.
20. R. L. Hoffman, A study of the advancing interface, *J. Colloid Interface Sci.* **50**, 228 (1975).
21. P. Sheng and M. Zhou, Immiscible-fluid dipslacement: Contact-line dynamics and the velocity-dependent capillary pressure, *Phys. Rev. A* **45**, 5694 (1992).
22. K. J. Ruschak, A method for incorporating free boundaries with surface tension in finite element fluid-flow simulation, *Int. J. Numer. Methods Fluids* **15**, 639 (1980).